SAND2015-9807J

Physically-based strength model of tantalum incorporating effects of temperature, strain rate and pressure

Hojun Lim,[1, a)] Corbett C. Battaile,[1] Justin L. Brown,[1] and Christopher R. Weinberger[2]
[1)] *Sandia National Laboratories, Albuquerque, NM 87185, USA*
[2)] *Drexel University, Philadelphia, PA 19104, USA*

(Dated: 23 October 2015)

In this work, we develop a tantalum strength model that incorporates effects of temperature, strain rate and pressure. Dislocation kink-pair theory is used to incorporate temperature and strain rate effects while the pressure dependent yield is obtained through the pressure dependent shear modulus. Material constants used in the model are parameterized from tantalum single crystal tests and polycrystalline ramp compression experiments. It is shown that the proposed strength model agrees well with the temperature and strain rate dependent yield obtained from polycrystalline tantalum experiments. Furthermore, the model accurately reproduces the pressure dependent yield stresses up to 250 GPa. The proposed strength model is then used to conduct simulations of a Taylor cylinder impact test and validated with experiments. This approach provides a physically-based multi-scale strength model that is able to predict the plastic deformation of polycrystalline tantalum through a wide range of temperature, strain and pressure regimes.

Keywords: Tantalum, strain rate, temperature, pressure, dynamic simulations, kink-pair theory

I. INTRODUCTION

Body-centered-cubic (BCC) metals, including tantalum, are well-known to exhibit strong temperature and strain rate dependent mechanical behaviors compared with close-packed structured metals[1,2]. Accurate materials modeling in these varying environments is especially important as tantalum has a wide variety of applications in extreme conditions, i.e. high temperature, strain rate and pressure. Several continuum models exist to describe the strongly temperature and strain-rate dependent flow behaviors of BCC metals[3–8]. Most of these classical models, i.e. Johnson-Cook (JC)[3,5] and Zerilli-Armstrong (ZA)[6], are empirical in form and their parameters are calibrated to experimental data of polycrystals at high temperatures and strain rates. More recently, the Mechanical Threshold Stress (MTS)[7,9], Steinberg-Guinan-Lund (SGL)[10,11] and Preston-Tonks-Wallace (PTW)[12] models have been proposed to account for thermal activation of dislocations. These models successfully reproduce the flow behavior of polycrystalline tantalum at temperatures of 25 - 1000 °C and strain rates of $\dot{\epsilon}$=10^{-4} -10^{4} s^{-1}. In addition to temperature and strain rate dependence, the SGL model incorporates pressure dependence while the PTW model considers different material behaviors in two different strain rate regimes to account for overdriven-shock ($\dot{\epsilon} = 10^{9} - 10^{12}$ s^{-1}). These models, however, are generally fit to macroscopic observables from polycrystalline experiments and do not consider the physics from lower length scale models/ experiments.

Dislocation kink-pair theory has been proposed to accurately model the motion of thermally activated screw dislocations in BCC metals and therefore describe these materials' temperature and strain rate dependent flow[13–17]. The theory has been used to successfully describe the temperature and strain rate dependence of various BCC single crystals, e.g. tantalum[14], molybdenum[18–20], tungsten[21,22], α-iron[23–25] and niobium[26]. Recently, this theory was used in meso-scale crystal plasticity models to incorporate temperature and strain rate dependent behaviors in BCC polycrystals[27,28].

In the present work, we extend the dislocation kink-pair model to develop an analytical strength model for tantalum that incorporates effects of temperature, strain rate and pressure. The proposed strength model is based on thermally activated dislocation physics and is parameterized by single crystal experiments and polycrystalline ramp compression experiments. The model is validated with experimental data from the literature. In addition, the model is implemented into Sandias solid dynamics software, ALEGRA[29], to simulate ballistic Taylor cylinder impact tests. The deformed shape from the Taylor cylinder simulations, based on this proposed tantalum strength model, agrees well with experimental data and should be amenable to various applications involving high temperature, strain rate and pressure.

II. DISLOCATION KINK-PAIR THEORY

Dislocation kink-pair theory assumes that the shear stress, τ, resolved onto the active slip system can be decomposed into thermal and athermal contributions:

$$\tau = \bar{\tau} + \tau^{*}\left(T, \dot{\gamma}\right). \tag{1}$$

Here, the first term, $\bar{\tau}$, is the athermal component of the flow stress that is attributed to long-range interactions. For example, $\bar{\tau}$ can be represented by using the forest

[a)] Electronic mail: hnlim@sandia.gov

dislocation density, ρ_f, as follows[30]:

$$\bar{\tau} = \alpha\mu b\sqrt{\rho_f}, \tag{2}$$

where, α is a material constant and μ is the shear modulus. $\bar{\tau}$ depends directly on the initial defect density, heat treatment and loading histories of the material. $\bar{\tau}$ can be obtained from single crystal experiments at high temperature ($T > T_c$) where the thermal part of the lattice friction becomes negligible. For example, a value of $\bar{\tau}$= 12 MPa was obtained for tantalum from single crystal cyclic tests at temperatures above 350 K[14]. The thermal

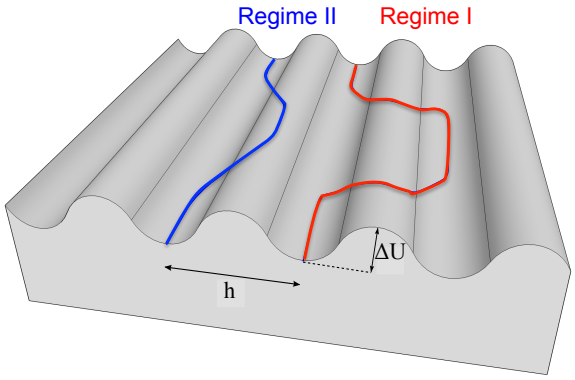

FIG. 1. Illustration of Peierls barrier and dislocation kink-pair at two temperature regimes. One dislocation shows a bulge in the line (on the left), described by the line tension model; and the second dislocation (right) has well formed kinks, described by the elastic interaction model. The valleys and peaks are separated by the spacing h and the height of the Peierls potential is ΔU.

part of the flow stress, τ^*, is attributed to strong temperature dependent lattice friction that requires thermal activation to overcome the Peierls barrier. Figure 1 shows a schematic of Peierls barrier and dislocation kink-pairs at two temperature and strain rate regimes. In the high temperature and low stress regime (Regime I), the dislocation kinks are fully formed and well separated (red dislocation line in Figure 1). Thus, the flow stress in Regime I can be represented using the elastic interaction (EI) model, τ^*_{EI}, as follows[13,31]:

$$\tau^*_{EI} = \tau^0_{EI}\left[1 - \left(\frac{k_B T \ln(\dot{\gamma}_0/\dot{\gamma})}{2H_k}\right)\right]^2. \tag{3}$$

Here, H_k is the formation enthalpy of an isolated kink, k_B is Boltzmann's constant, $\dot{\gamma}_0$ is the reference shear rate, and τ^0_{EI} is the material parameter representing τ^*_{EI} at 0 K.

In the low temperature and high stress regime (Regime II), the dislocation kinks are not fully formed (blue dislocation line in Figure 1). The flow stress in Regime II can be obtained from a dislocation line tension (LT) model. To evaluate the LT model, a numerical representation of the Peierls barrier must be assumed. For the antiparabolic representation of the Peierls potential, the flow stress in Regime II can be represented as follows[17,32,33]:

$$\tau^*_{LT} = \tau^0_{LT}\left[1 - \left(\frac{k_B T \ln(\dot{\gamma}_0/\dot{\gamma})}{2H_k}\right)^{1/2}\right], \tag{4}$$

where τ^0_{LT} is a material parameter that represents τ^*_{LT} at 0 K. Using this double regime dislocation-based strength model, τ^* at different temperatures and strain rates can be determined from[13]:

$$\tau^* = \min\left(\tau^*_{EI}, \tau^*_{LT}\right). \tag{5}$$

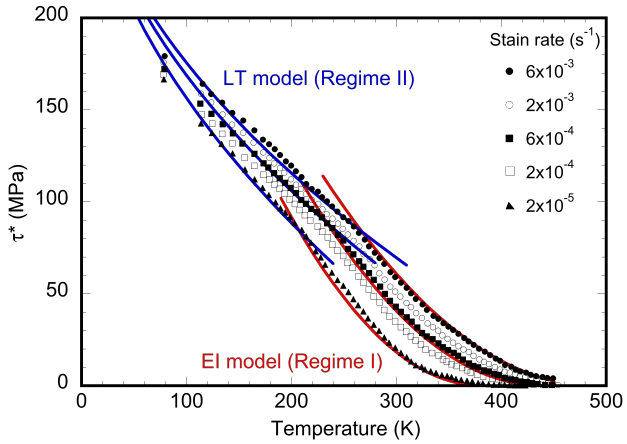

FIG. 2. Measured (data points) and calibrated (solid lines) τ^* of single crystal tantalum at different temperatures and strain rates using the EI and LT models[14,27]. Here, the fits are for the highest, lowest and middle strain rates.

The kink-pair model in Equation (5) was fit to tantalum single crystal experiments at various temperatures and strain rates[14]. Here, experimental values of τ^* are obtained via the Ackermann-Mughrabi technique and using pre-deformed specimens that have a stable dislocation cell structure to minimize the variance in the observed response[14,26]. Figure 2 compares measured and fitted τ^* of tantalum single crystals at different temperatures and strain rates using the dislocation kink-pair model[27]. The model accurately captures temperature and strain rate dependent flow behavior of tantalum single crystals. The best-fit material parameters used in the model are listed in Table I[27].

III. P AND T DEPENDENT SHEAR MODULUS

Conventional strength models that incorporate dislocation plasticity do not generally consider the effect of pressure on yield. However, in extremely high pressure regimes, pressure influences the shear modulus and hence the flow behavior of tantalum[34–36]. Some constitutive

TABLE I. Best-fit material parameters for tantalum strength model fit from tantalum single crystal experiments and polycrystalline ramp compression tests[10,14,27,34].

Equations	Parameters	Values
Eqns. (3)-(4)	$\dot{\gamma}_0$	2.99×10^6 s^{-1}
	$2H_k$	0.85 eV
	τ^0_{EI}	406 MPa
	τ^0_{LT}	320 MPa
Eqn. (7)	μ_0	69 GPa
	μ'_T	0.009 GPa/K
	α_1	7.9907×10^{-1} GPa^{-1}
	α_2	2.1292×10^{-3} GPa^{-2}

models have been proposed to relate pressure to the shear modulus from both experiments and lower length-scale simulations[10,37]. In this work, the pressure dependent shear modulus is calibrated to high-rate ramp compression experiments (3×10^5 s^{-1}) at room temperature up to 250 GPa using Z pulsed power facility at Sandia National Laboratories[34].

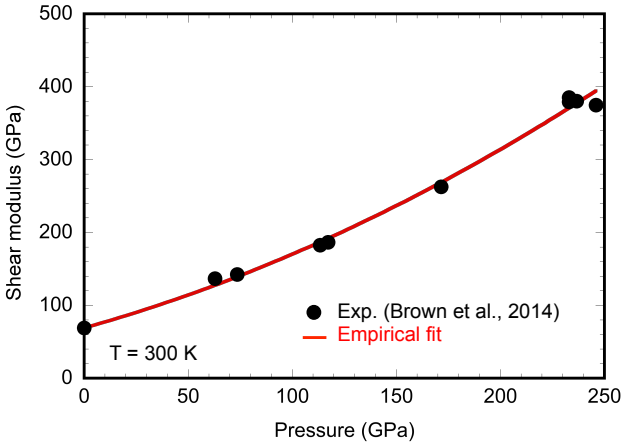

FIG. 3. Pressure dependent shear modulus of polycrystalline tantalum from the ramp compression experiments (data points)[34] and polynomial fit (solid line). The ramp compression tests were conducted at the strain rate of 3×10^5 s^{-1} and 300 K.

Figure 3 shows a plot of the measured (data points) and calibrated (solid line) pressure dependent shear modulus. Note that in contrast to conventional models[10], there is a non-linear relation between the shear modulus and the pressure. The following polynomial was used to represent the pressure dependent shear modulus:

$$\mu(P) = \mu_0 + \alpha_1 P + \alpha_2 P^2, \tag{6}$$

where μ_0 is the shear modulus at the reference state (T=0 K and P=0) and, α_1 and α_2 are the fitting parameters.

Note that the shear modulus is dependent on both the temperature and the pressure. The shear modulus is reported to be nearly linear in temperature up to the melting point[38]. By incorporating both the temperature and pressure effects, the shear modulus can be written as follows:

$$\mu(P,T) = \mu_0 - \mu'_T\,(T-300) + \alpha_1 P + \alpha_2 P^2, \tag{7}$$

where μ'_T is the derivative of the shear modulus with respect to temperature. Table I lists the best-fit parameters in Equation (7) that were used to create the red line in Figure 3[10].

IV. STRENGTH MODEL INCORPORATING T, $\dot{\gamma}$ AND P

The Arrhenius law relates the rate of plastic deformation, $\dot{\gamma}$, to the activation enthalpy and temperature as follows:

$$\dot{\gamma} = \dot{\gamma}_0 \exp\left(\frac{-\Delta H}{k_B T}\right), \tag{8}$$

where ΔH is the activation enthalpy. ΔH can be represented using the ratio of the resolved shear stress (τ) and the Peierls stress (τ_p) as follows[39]:

$$\Delta H = \Delta H_0 \left(1 - \left(\frac{\tau^*}{\tau_p}\right)^p\right)^q, \tag{9}$$

where p and q are parameters that determine the shape of the energy barrier profile such that $0 \le p \le 1$ and $1 \le q \le 2$ are satisfied. Note that when $p = 0.5$ and $q = 1$, the activation enthalpy law is in the same form as the EI model and when $p = 1$ and $q = 2$ the law corresponds to the LT model.

It has been shown that τ_p and ΔH_0 are proportional to shear modulus such that the following relations are satisfied[9,40]:

$$\tau_p = \frac{\mu}{\mu_0}\tau_p^0, \tag{10}$$

$$\Delta H_0 = \frac{\mu}{\mu_0}\Delta H_0^0, \tag{11}$$

where τ_p^0 and ΔH_0^0 represents reference states of the Peierls stress and the activation enthalpy, respectively.

Thus, the general form of τ^* that depends on the current μ can be written as follows:

$$\tau = \frac{\mu}{\mu_0}\tau_p^0 \left[1 - \left(\frac{\mu_0 k_B T \ln(\dot{\gamma}_0/\dot{\gamma})}{\mu \Delta H_0^0}\right)^{1/q}\right]^{1/p}. \tag{12}$$

The form in Equation (12) can then be applied to the two kink-pair models, the LT and EI models, in Equations (3) and (4) as follows:

$$\tau^*_{EI} = \frac{\mu}{\mu_0}\tau^0_{EI} \left[1 - \left(\frac{\mu_0 k_B T \ln(\dot{\gamma}_0/\dot{\gamma})}{\mu(2H_k^0)}\right)\right]^2, \tag{13}$$

$$\tau^*_{LT} = \frac{\mu}{\mu_0}\tau^0_{LT}\left[1 - \left(\frac{\mu_0 k_B T \ln(\dot{\gamma}_0/\dot{\gamma})}{\mu(2H^0_k)}\right)^{1/2}\right]. \quad (14)$$

Here, $2H^0_k$ is the kink activation enthalpy at the reference state. In addition, the athermal part of the flow stress, $\bar{\tau}$, in Equation (15) also depends on the shear modulus and can be represented as follows:

$$\bar{\tau} = \frac{\mu}{\mu_0}\bar{\tau}_0, \quad (15)$$

where $\bar{\tau}_0$ is the athermal stress at the references state.

The shear stress of a single crystal resolved onto the active slip system (τ) can be related to the uniaxial stress applied to a polycrystal (σ), as follows:

$$\sigma = \bar{M}\tau, \quad (16)$$

where $\bar{M}$ is the average Taylor factor that represents the ratio between the macroscopic stress and the resolved shear stress. For BCC polycrystals, $\bar{M}$ ranges between 2.733 to 3.067, depending on the specific slip systems[41–46]. In this work, we use $\bar{M}$ value of 3.06 for $\{110\}\langle 111\rangle$ slip.

Using Equations (1) and (16), the yield stress of polycrystalline tantalum (σ_y) can be represented as follows:

$$\sigma_y = \bar{M}\left[\bar{\tau} + \min(\tau^*_{EI}, \tau^*_{LT})\right]. \quad (17)$$

Note that in Equation (17), both $\bar{\tau}$ and τ^* depend on pressure and temperature while the only latter term is affected by the strain rate.

Figures 4 (a) and (b) compare the measured and predicted yield stresses of polycrystalline tantalum at different strain rates and temperatures. In Figure 4 (a), the strain rate dependent yield stress is calculated using the model developed here and compared with the measured yield stress at 300 K[9,27,47–50]. Similarly, the predicted temperature dependence is compared with experimental data at constant strain rate of 10^{-4} s^{-1}[47,50]. It is shown that the model agrees reasonably well with various experimental measurements from the literature and it is within the scatter of the experimental data. The model predictions in Figures 4 (a) and (b) show a transition between the two models, EI and LT, with varying temperature and strain rate. The model calibrated from single crystal data accurately predict polycrystalline behavior within a strain-rate range of 10^{-6} - 10^4 s^{-1} and a temperature range of 0 - 500 K.

Figure 5 shows pressure dependence on the yield stresses of polycrystalline tantalum. Experimental data are obtained from ramp compression of tantalum at a nominal strain rate of 3×10^5 s^{-1} at room temperature[34]. The measured pressure dependence is compared with our model and with the SG[10], PTW[12], SGL[11] and LM[37] models. Here, $\bar{\tau}$ = 91 MPa is used to fit the measured yield stress of cold rolled tantalum plate at 62 GPa. It is shown that our model captures pressure dependence of polycrystalline tantalum reasonably well, especially at high pressures, as compared to other existing models. All

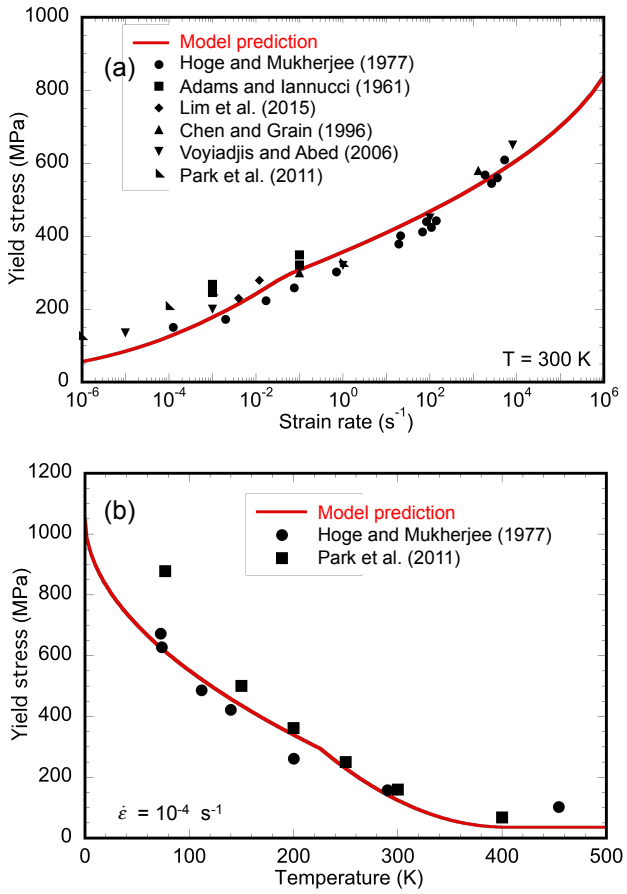

FIG. 4. (a) Measured[9,27,47–50] and predicted yield stresses of polycrystalline tantalum for different strain rates at 300 K and (b) measured[47,50] and predicted yield stresses of polycrystalline tantalum for different temperatures at $\dot{\epsilon} = 10^{-4}$ s^{-1}

four of the existing models from the literature predict a nearly linear pressure dependence and tend to underpredict the measured values at high pressures. This may be attributed to the fact that these models are fit to lower pressure regimes, i.e. less than 100 GPa.

V. DYNAMIC SIMULATION OF TAYLOR IMPACT TEST

The constitutive model described in the previous section was used in high-rate simulations of a common benchmark application: Taylor cylinder impact tests of a projectile specimen impinging on a hard target[51]. This method is often used to validate solid dynamics simulation codes and models and it provides a simple, convenient, and robust approach for subjecting a single specimen to a wide range of strain rates across its length.

The simulation was conducted using ALEGRA, a Lagrangian-Eulerian multi-physics code developed at

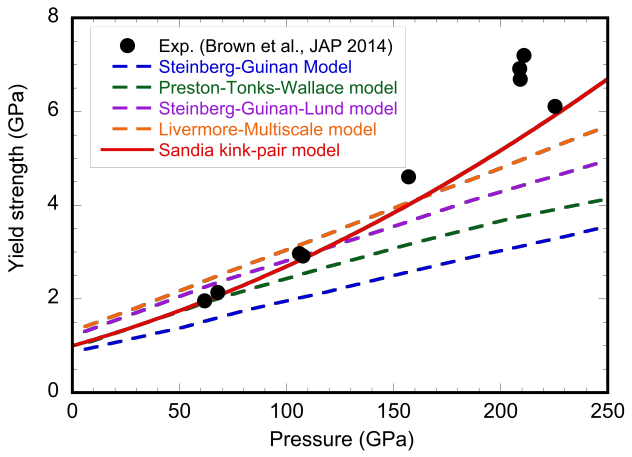

FIG. 5. Pressure dependence of polycrystalline tantalum from ramp experiments[34] and various strength models. The proposed strength model agrees reasonably well with the Z ramp experiments compared to other existing models[10–12,37].

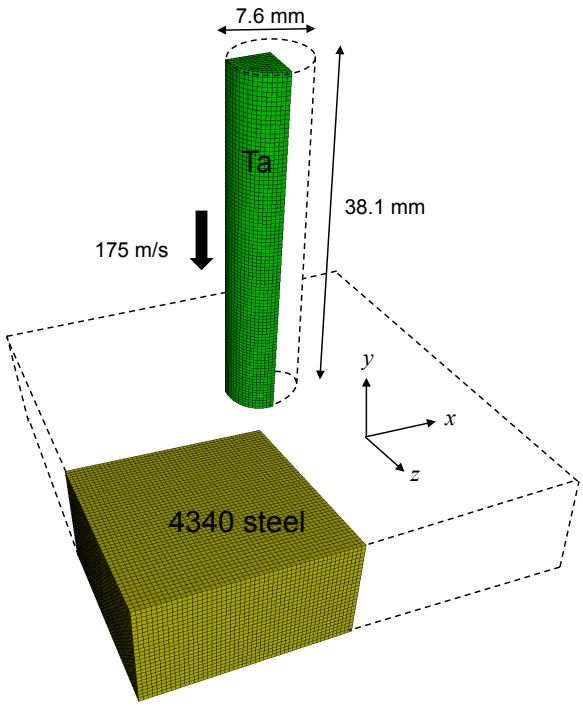

FIG. 6. A schematic of a Taylor cylinder impact test. Tantalum cylinder impinges on 4340 steel block at a velocity of 175 m/s.

Sandia National Laboratories. Figure 6 shows a schematic of a Taylor impact test. The simulated projectile is a tantalum cylinder with dimensions of 38.1 mm in length and 7.62 mm in diameter, and impinges upon a hard surface of 4340 steel at a velocity of 175 m/s. The simulation was conducted at standard atmospheric conditions described by a temperature of 298 K and pressure of 1 bar.

The three-dimensional Lagrangian simulations were conducted with 9,120 hexahedral finite elements in the tantalum projectile, and a target surface consisting of a block of 4340 steel described by 62,500 hexahedral finite elements. A three-dimensional quarter-symmetry condition is used for efficiency. The MESQUITE remeshing algorithm was imposed at every time step in the ALEGRA simulations to avoid numerical artifacts associated with ill-conditioned finite elements evolving during deformation. The contact between the projectile and target was assumed to be frictionless.

In ALEGRA, each material requires models for the equation of state (EOS) and the elastic-plastic deformation (strength model). For the tantalum projectile and the steel plate, a Mie-Grüneisen EOS model and Sesame tabular EOS data were used to represent the EOS of each material, respectively[52]. For the strength model of tantalum, the LT portion of the dislocation kink-pair model, which is suitable for the high rate regime in Equation (4), was used. The strain hardening rate is represented by an empirical law using tanh function as follows[53]:

$$\frac{\partial \sigma}{\partial \epsilon_p} = \theta_0 \left(1 - \frac{\tanh\left(\alpha\sigma/\sigma_s\right)}{\tanh(\alpha)}\right), \tag{18}$$

where ϵ_p is the equivalent plastic strain, θ_0 and α are the material parameters and σ_s represent temperature and strain rate dependent saturation stress that can be represented as follows[54]:

$$\sigma_s = \sigma_s^0 \left(\frac{\dot{\gamma}}{\dot{\gamma}_0^s}\right)^{\frac{k_B T}{\mu b^3 A}}, \tag{19}$$

where, A, α and $\dot{\gamma}_0^s$ are material constants.

For the 4340 steel, a Zerilli-Armstrong yield model having the following form was used[6].

$$\sigma_Z = C_1 + C_2 \exp\left(-C_3 T + C_4 T \ln \dot{\epsilon}_p\right) + C_5 \epsilon_p^N, \tag{20}$$

where, C_1 - C_5 and N are material parameters. Table II lists material parameters used in yield models for tantalum and 4340 steel.

Figure 7 (a) compares the measured[55] and simulated shape of the tantalum projectile after impact under the same conditions. The simulated image was captured after the projectile reflected off the steel plate such that the center-point of the bottom of the (deformed) specimen reached its initial position of approximately 0.1 mm above the target surface. The simulated specimen shape shows relatively good agreement with the measurement.

The profiles of the projectile's shapes after impact are shown in Figure 7 (b), which contains the x-y coordinates along the outer surface from the ALEGRA simulation and previously published experiments on tantalum Taylor impact tests[55]. The simulation predictions agree well with the experiments. The total lengths of the de-

TABLE II. Material parameters used in ALEGRA Taylor impact tests for tantalum and 4340 steel. Any parameters not listed in the table were left at their default values.

Materials	Parameters	Values
Tantalum	σ_s^0	575 GPa
	$\dot{\gamma}_0^s$	10^7 s^{-1}
	θ_0	2 GPa
	b	2.86 Å
	α	2.75
	A	1.6
4340 steel	C_1	89.8 MPa
	C_2	2.07 GPa
	C_3	17.4 K^{-1}
	C_4	0.56 K^{-1}
	C_5	1.03 GPa
	N	0.531

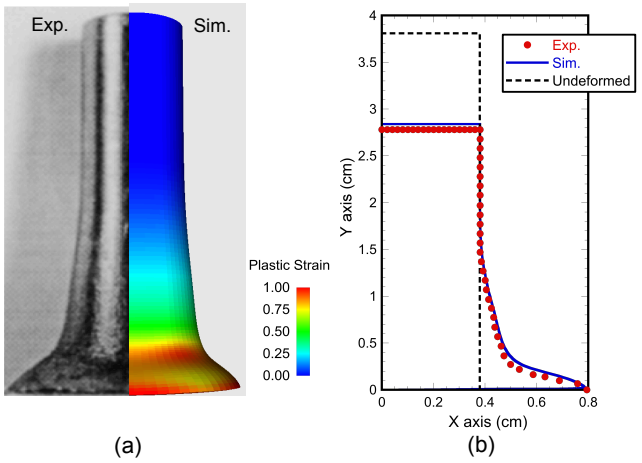

FIG. 7. (a) Specimen shapes and equivalent plastic strain maps predicted by ALEGRA simulations of impact of a three-dimensional, quarter-symmetric tantalum specimen into a 4340 steel plate and (b) Projectile shape profiles (not to scale) predicted by ALEGRA simulations, with results reported from earlier Taylor cylinder impact experiments[55] (using the measurements from the minor axis).

formed projectile was 28.4 mm from the simulation and 27.8 mm from the experiment, deviating approximately 2 %. This discrepancy could arise from a variety of factors, including the lack of crystallographic texture, plastic anisotropy, and deformation twinning[56,57] in the simulated projectile; and the frictionless contact between the projectile and the target.

VI. CONCLUSIONS

In this work, we introduced a multi-scale model of plasticity in pure tantalum that captures temperature, strain rate and pressure effects on material strength. The basis of this model is fundamental dislocation mechanics, specifically kink-pair theory which accurately captures the strain rate and temperature dependence of yield. These results provide an example of a multi-scale integration of simulations and experiments from the dislocation scale, through the meso- and micro-scales, and into macro-scale continuum solid dynamics. The use of the multi-scale strength model to simulate Taylor impact experiments, and its close agreement with measured deformation profiles demonstrates the utility and robustness of this model.

ACKNOWLEDGMENTS

Sandia National Laboratories is a multi-program laboratory managed and operated by Sandia Corporation, a wholly owned subsidiary of Lockheed Martin Corporation, for the U.S. Department of Energy's National Nuclear Security Administration under contract DE-AC04-94AL85000.

[1] J. W. Christian, "Some surprising features of the plastic deformation of body-centered-cubic metals and alloys," Met. Trans. A **14A**, 1237–1256 (1983).
[2] G. Taylor, "Thermally-activated deformation of BCC metals and alloys," Prog. Mater. Sci. **36**, 29–61 (1992).
[3] G. R. Johnson and W. J. Cook, "A constitutive model and data for metals subjected to large strains, high strain rates and high temperatures," Seventh International Symposium on Ballistics, The Hague, The Netherlands , 541–547 (1983).
[4] L. Anand, "Constitutive equations for hot working of metals," Int. J. Plasticity **1**, 213–231 (1985).
[5] G. R. Johnson and W. H. Cook, "Fracture characteristics of three metals subjected to various strains, strain rates, temperatures and pressures," Eng. Fract. Mech. **21**, 31–48 (1985).
[6] F. J. Zerilli and R. W. Armstrong, "Dislocation-mechanics-based constitutive relations for material dynamics calculations," J. Appl. Phys. **61**, 1816–1825 (1987).
[7] P. S. Follansbee and U. F. Kocks, "A constitutive description of the deformation of copper based on the use of the mechanical threshold stress as an internal state variable," Acta metall. **1**, 81–93 (1988).
[8] A. S. Khan and R. Liang, "Behaviors of three bcc metal over a wide range of strain rates and temperatures: experiments and modeling," Int. J. Plasticity **15**, 1089–1109 (1999).
[9] S. R. Chen and G. T. Gray, "Constitutive behavior of tantalum and tantalum-tungsten alloys," Met. Mater. Trans. A **27**, 2994–3005 (1996).
[10] D. J. Steinberg, S. G. Cochran, and M. W. Guinan, "A constitutive model for metals applicable at high-strain rate," Journal of Applied Physics **51**, 1498–1504 (1980).
[11] D. J. Steinberg and C. M. Lund, "A constitutive model for strain rates from 10^{-4} to 10^{-6} s^{-1}," Journal of Applied Physics **65**, 1528–1533 (1989).
[12] D. L. Preston, D. L. Tonks, and D. C. Wallace, "Model of plastic deformation for extreme loading conditions," Journal of Applied Physics **93**, 211–220 (2003).
[13] A. Seeger, "The temperature and strain-rate dependence of the flow stress of body-centered cubic metals: A theory based on kink–kink interactions," Z. Metallikd **72**, 369–380 (1981).
[14] M. Werner, "Temperature and strain-rate dependence of the flow stress of ultrapure tantalum single crystal," Phys. Status Solidi A **104**, 63–78 (1987).
[15] A. Seeger, "Why anomalous slip in body-centred cubic metals?" Mater. Sci. Eng. A **319-321**, 254–260 (2001).

[16]M. Z. Butt, "Kinetics of flow stress in crystals with high intrinsic lattice friction," Philos. Mag. **87**, 3595–3614 (2007).
[17]A. Argon, *Strengthening mechanisms in crystal plasticity* (Oxford University Press, 2008).
[18]A. Seeger, "The flow stress of high-purity refractory body-centered cubic metals and its modification by atomic defects," Journal de Physique IV **5**, C7–45–C7–65 (1995).
[19]L. Hollang, M. Hommel, and A. Seeger, "The flow stress of ultra-high-purity molybdenum single crystals," Phys. Status Solidi A **160**, 329–354 (1997).
[20]L. Hollang, D. Brunner, and A. Seeger, "Work hardening and flow stress of ultrapure molybdenum single crystals," Mater. Sci. Eng. A **319**, 233–236 (2001).
[21]D. Brunner and V. Glebovsky, "Analysis of flow-stress measurements of high-purity tungsten single crystals," Mat. Lett. **42**, 144–152 (2000).
[22]D. Brunner and V. Glebovsky, "The plastic properties of high-purity W single crystals," Mat. Lett. **42**, 290–296 (2000).
[23]D. Brunner and J. Diehl, "Strain-rate and temperature dependence of the tensile flow stress of high-purity α-iron above 250 K (regime I) Studied by means of stress-relaxation tests," Phys. Status Solidi A **124**, 155–170 (1991).
[24]D. Brunner and J. Diehl, "Temperature and strain-rate dependence of the tensile flow stress of high-purity α-iron below 250 K I. stress/temperature regime III," Phys. Status Solidi A **124**, 355–464 (1991).
[25]D. Brunner and J. Diehl, "Temperature and strain-rate dependence of the tensile flow stress of high-purity α-iron below 250 K II. stress/temperature regime II and its transitions to regimes I and iii," .
[26]F. Ackermann, H. Mughrabi, and A. Seeger, "Temperature- and strain-rate dependence of the flow stress of ultrapure niobium single crystals in cyclic deformation," Acta. Metall. **31**, 1353–1366 (1983).
[27]H. Lim, C. C. Battaile, J. D. Carroll, B. L. Boyce, and C. R. Weinberger, "A physically based temperature and strain rate dependent crystal plasticity model for bcc metals," J. Mech. Phys. Sol. **74**, 80–96 (2015).
[28]H. Lim, L. M. Hale, Z. A. Zimmerman, C. C. Battaile, and C. R. Weinberger, "A multi-scale model of dislocation plasticity in α-Fe: Incorporating temperature, strain rate and non-schmid effects," Int. J. Plasticity **73**, 100–118 (2015).
[29]ALEGRA, http: //www.cs.sandia.gov/ALEGRA/Alegra_Home.html.
[30]G. I. Taylor, "The mechanism of plastic deformation of crystals. Part I. Theoretical," Proc. Roy. Soc. A **165**, 362–387 (1934).
[31]J. Hirth and J. Lothe, *Theory of Dislocations* (Krieger, 1982).
[32]J. E. Dorn and S. Rajnak, "Nucleation of kink pairs + Peierls mechanism of plastic deformation," Transactions of the Metallurgical Society of AIME **230**, 1052 (1964).
[33]D. Caillard and J. L. Martin, *Thermally activated mechanisms in crystal plasticity* (Pergamon, 2003).
[34]J. Brown, C. Alexander, J. Asay, T. J. Vogler, D. H. Dolan, and J. L. Belof, "Flow strength of tantalum under ramp compression to 250 gpa," Journal of Applied Physics **115**, 043530 (2014).
[35]A. Dewaele and P. Loubeyre, "Mechanical properties of tantalum under high pressure," Physical Review B **72**, 134106 (2005).
[36]J. R. Asay, T. Ao, T. J. Vogler, J. P. Davis, and G. T. G. III, "Yield strength of tantalum for shockless compression 18 gpa," Journal of Applied Physics **106**, 073515 (2009).
[37]N. R. Barton, J. V. Bernier, R. Becker, A. Arsenlis, R. Cavallo, J. Marian, M. Rhee, H. S. Park, B. A. Remington, and R. T. Olson, "A multiscale strength model for extreme loading conditions," Journal of Applied Physics **109**, 073501 (2011).
[38]D. Steinberg, "Constitutive model used in computer simulation of time-resolved, shock-wave data," International Journal of Impact Engineering **5**, 1–4 (1997).
[39]U. F. Kocks, A. S. Argon, and M. F. Ashby, "Thermodynamics and kinetics of slip," Progress in Materials Science **19**, 1–289 (1975).
[40]C. R. Weinberger, G. J. Tucker, and S. Foiles, "The Peierls potential of screw dislocations in bcc transition metals: predictions form density functional theory," Phys. Rev. B **87**, 054114 (2013).
[41]G. I. Taylor, "Plastic strain in metals," J. Inst. Metals **62**, 307–324 (1938).
[42]J. W. Hutchinson, "Plastic deformation of b.c.c. polycrystals," Journal of the Mechanics and Physics of Solids **12**, 25–33 (1964).
[43]G. Y. Chin and W. L. Mammel, "Computer solutions of the Taylor analysis for axisymmetric flow," Trans. Metall. Soc. AIME **239**, 1400–1405 (1967).
[44]U. F. Kocks, "The relation between polycrystal deformation and single-crystal deformation," Met. Trans. B **1**, 1121–1143 (1970).
[45]J. Rosenberg and H. Piehler, "Calculation of the taylor factor and lattice rotations for bcc metals deforming by pencil glide," Metallurgical Transactions **2**, 257–259 (1971).
[46]R. Stoller and S. Zinkle, "On the relationship between uniaxial yield strength and resolved shear stress in polycrystalline materials," Journal of nuclear materials **287**, 349–352 (2000).
[47]K. G. Hoge and A. K. Mukherjee, "The temperature and strain rate dependence of the flow stress of tantalum." J. Mat. Sci. **12**, 1666–1672 (1977).
[48]M. A. Adams and A. Iannucci, "The mechanical properties of tantalum with special reference to the ductile-brittle transition," ASD Technical Report , 61–203 (1961).
[49]G. Z. Voyiadjis and F. H. Abed, "A coupled temperature and strain rate dependent yield function for dynamic deformations of bcc metals," Int. J. Plasticity **22**, 1398–1431 (2006).
[50]C. H. Park, S. G. Hong, and C. S. Lee, "A unified constitutive model for quasi-static flow responses of pure ta and ta-w alloys," Mat. Sci. Eng. A **528**, 1154–1161 (2011).
[51]G. Taylor, "The use of flat-ended projectiles for determining dynamic yield stress. I. theoretical considerations," Proceedings of the Royal Society of London A **194**, 289–299 (1948).
[52]G. I. Kerley, "CTH reference manual: The equation of state package," Technical report SAND98-0947, Sandia National Laboratories, Albuquerque, NM (1998).
[53]D. M. Goto, J. F. Bingert, S. R. Chen, G. T. G. III, and R. K. Garrett, "The mechanical threshold stress constitutive-strength model description of HY-100 steel," Metallurgical and Materials Transactions A **31**, 1985–1996 (2000).
[54]U. F. Kocks, "Laws for work-hardening and low-temperature creep," J. Eng. Mater. Tech., ASME **98**, 76–85 (1976).
[55]P. J. Maudlin, J. F. Bingert, J. W. House, and S. R. Chen, "On the modeling of the Taylor cylinder impact test for orthotropic textured materials: experiments and simulations," International Journal of Plasticity **15**, 139–166 (1999).
[56]L. E. Murr, M. A. Meyers, C. S. Niou, Y. H. Chen, S. Pappu, and C. Kennedy, "Shock-induced deformation twinning in tantalum," Acta materialia **45**, 157–175 (1997).
[57]C. Q. Chen, G. Hu, J. N. Florando, M. Kumar, K. J. Hemker, and T. K. Ramesh, "Interplay of dislocation slip and deformation twinning in tantalum at high strain rates," Scripta Materialia **69**, 709–712 (2013).